International Journal of Safety and Security Engineering
Vol. 15, No. 11, November, 2025, pp. 2239-2246
Journal homepage: http://iieta.org/journals/ijsse

Influence of Grain Size Distribution of Sand Lenses in Evaluating the Liquefaction Potential

Putera Agung Maha Agung[1*], Suripto[1], Denny Yatmadi[1], Satwarnirat[2], Syaiful Amri[2], Muhammad Fathur Rouf Hasan[3]

[1] Department of Civil Engineering, Politeknik Negeri Jakarta, Depok 16425, Indonesia
[2] Department of Civil Engineering, Politeknik Negeri Padang, Padang 25164, Indonesia
[3] Graduate School, Universitas Brawijaya, Malang 65145, Indonesia

Corresponding Author Email: putera.agungmagung@sipil.pnj.ac.id

https://doi.org/10.18280/ijsse.151105

Received: 24 October 2025
Revised: 25 November 2025
Accepted: 28 November 2025
Available online: 30 November 2025

Keywords:
earthquake, liquefaction, loose sand lenses, grain size, immediate settlement, pore water pressure

ABSTRACT

Sand lenses are susceptible to ground motion due to dynamic loads like earthquakes. Infrastructure can be damaged by liquefaction that occurs in saturated sand lenses. A study on the safety factor (SF) of liquefaction potential and immediate settlement (ΔS_e) was carried out at an area of infrastructure development in Langsa, Indonesia. This region features many alluvial deposits, which have multiple fine to coarse sand lenses from loose to medium conditions and varying in thickness from 2.0 to 3.0 m. This research aims to evaluate the effect of grain size distribution (GSD) on sand lenses susceptible to liquefaction, as well as the extent of immediate land subsidence following liquefaction. Laboratory analysis of GSD allows for the calculation of the uniformity coefficient (C_u), fines content (FC), and curvature coefficient (C_c). It also helps in assessing the likelihood of liquefaction potential and ΔS_e within the sand lens layer. The laboratory analysis conducted by GSD revealed that at the vulnerable sand lens layers situated 2.0 to 10.0 m beneath the current groundwater table, C_u value of 13 and C_c value of 0.31 were recorded, while the FC value was approximately 2%. This indicates an increased liquefaction potential as the SF diminishes. Prediction of SF values existed in the range from 0.66 to 1.49 and ΔS_e from 2.12 to 88.07 mm. Probability of liquefaction (P[L]) existed in the range from 0% to 30%, with pore water pressure (u) reaching until 35% from the hydrostatic pressure during liquefaction.

1. INTRODUCTION

One of the regions with the highest seismic activity is Indonesia, which is situated at the meeting point of three main tectonic plates. This condition places many areas in Indonesia at high risk of natural disasters, including the phenomenon of soil liquefaction, which can trigger widespread and sudden infrastructure damage. Liquefaction events accompanied by land subsidence have occurred several times in Indonesia, such as during the 2018 Palu earthquake, which showed the destructive impact of extreme soil liquefaction [1]. According to conventional theory, liquefaction in sandy soil that is saturated or partially saturated results from cyclic (seismic) loads that cause the soil's mechanical resistance to decrease. The loss of effective stress between sandy soil particles ($\sigma' = 0$) in response to an applied stress is characterized by the increase in pore water pressure (u) to surpass the "overburden pressure" value ($u = \sigma$; $\Delta u = \sigma'$) in a saturated soil ($S_r = 100\%$) in a saturated soil ($S_r = 100\%$) under "undrained or short term" conditions [2].

The higher structures or foundations sink or tilt due to liquefaction, which occurs when the underlying soil loses its strength and is more liquid-like [3]. One of the critical consequences of liquefaction is ground settlement, which can be immediate and severely affect infrastructure stability and integrity [4]. One geological factor that can increase the risk of sudden liquefaction and land subsidence is the presence of sand lenses - layers of sand that are trapped discontinuously between fine-grained soils [5]. These sand lenses are local but very susceptible to liquefaction, especially when saturated with water. Due to their limited size and varied locations, sand lenses are often overlooked in conventional soil investigations. As a result, the risk of local and sudden subsidence is not properly identified.

As soon as the extra pore water pressure is released after a liquefaction event, the soil particles reorganize and densify, causing fast settlement. Buildings, pipelines, and transportation infrastructure are particularly susceptible to settlement ground lowering caused by this fast deformation. Sand lenses are localized, often thin, sandy layers embedded within finer-grained soils such as silts or clays [6]. Due to their high permeability and low cohesion, sand lenses are highly susceptible to liquefaction. Even if the surrounding soil is relatively stable, these lenses can initiate liquefaction and act as failure planes or weak zones during seismic events. Understanding the risk posed by sand lenses is crucial for accurately predicting ground behavior during and after seismic loading. Ignoring the settlement potential of these discrete sandy layers can lead to an underestimation of deformation and associated damage in geotechnical designs [7]. Hence,

assessing the immediate settlement (ΔS_e) caused by liquefiable sand lenses helps engineers and planners mitigate risks, improve soil models, and design safer infrastructure [8]. This leads to analyzing the ΔS_e during or shortly after the shaking. Sand lenses are especially critical because they liquefy quickly. Seismic waves cause the ground to undergo fast cyclic loading during an earthquake. This loading causes excess pore water pressure at these layers in saturated, loose, cohesionless soils such as sand lenses. The processes that result in fast or ΔS_e are as follows [9].

Seismic shaking induces soil particles in a saturated sandy soil to reorganize into a denser particle structure. Effective stress (the stress borne by the soil skeleton) falls, and pore water pressure rises due to water filling the voids and becoming hard to move during fast shaking. The effective stress decreases to almost zero as the pore pressure gets closer to the total vertical stress, and the soil rapidly exhibits liquid-like characteristics (liquefaction). During liquefaction, the soil loses its ability to resist shear stresses. This results in immediate deformation or settlement under the weight of structures or the overburden soil, as the soil grains lose interlocking and rearrange into a denser state. Once shaking stops, excess pore pressures dissipate, and water starts to drain from the soil. Effective stress gradually increases as water drains, and the soil particles settle further. A significant portion of ΔS_e occurs during or shortly after the shaking, especially in thin, loose, saturated sand lenses, which can quickly densify and collapse under gravity. Thin sand lenses, being highly permeable and low in cohesion, are particularly susceptible to liquefaction. Their limited thickness allows rapid pore pressure buildup and dissipation, resulting in quick settlement even before surrounding soils respond. These lenses can act as localized zones of weakness, where settlement is concentrated immediately after the earthquake. Earthquakes induce ΔS_e through cyclic loading, continuing to pore pressure buildup [10]; temporary loss of effective stress and shear strength; rapid densification and deformation during or right after shaking [11]. Sand lenses amplify this effect due to their physical and hydraulic properties, making them critical zones for early settlement detection and modeling.

Existing liquefaction models do not fully account for the behavior of thin sand lenses, which may lead to underestimation of ΔS_e risks during earthquakes. Most models and field assessments focus on large homogeneous sandy layers, not interbedded or lens-like sand deposits. To improve the understanding and prediction of ΔS_e caused by localized liquefaction in sand lenses. This research aims to evaluate the effect of grain size distribution (GSD) on sand lenses susceptible to liquefaction, as well as the extent of immediate land subsidence following liquefaction. This study quantifies the presence, thickness, and distribution of sand lenses within layered soil profiles contributing to local deformation, with the primary goal of improving the accuracy of liquefaction hazard assessments and providing more reliable information for geotechnical design practices in seismically active areas. ΔS_e theory: after liquefaction, soil particles reorient and densify. This leads to ΔS_e during or shortly after the shaking. Sand lenses are especially critical because they liquefy quickly due to saturation and permeability value. Their localized settlement can cause differential deformation [12].

2. BASIC THEORY

The basic theoretical foundation of liquefaction hazards related to sandy soil is grounded in principles of soil mechanics, effective stress theory, and cyclic loading behavior [13]. Below is a concise breakdown of the core theories. Classical theory from the effective stress principle (Terzaghi's principle): this theory is the foundation of soil behavior under load. Effective stress σ' is the stress actually carried by the soil skeleton:

$$\sigma' = \sigma - u \tag{1}$$

where, σ = total stress; u = pore water pressure. This theory is very relevant to the liquefaction process. Pore water pressure u rises during an earthquake due to cyclic loading. If u becomes nearly equal to σ, then $\sigma' \approx 0$, meaning the soil loses strength and behaves like a fluid (liquefaction). Cyclic loading and soil behavior: repeated shear stresses (cyclic loading) are applied to the soil during earthquakes. Loose saturated sands are especially susceptible because they will contract under loading; They have a slow rate of pore pressure dissipation, which leads to a rapid accumulation of excess pore water pressure. The likelihood of liquefaction depends on the number of cycles, the amplitude of shear stress, and the density of the soil.

Liquefaction is most common in loose, clean sands; silty sands; and sandy fills or reclaimed land. These soils have high porosity, low cohesion, and low permeability (like silty sands). Denser sands and well-graded soils are less susceptible because they can resist rearrangement under ground shaking due to an earthquake. Several empirical techniques based on field testing are frequently employed, particularly for calculating the cyclic resistance ratio (CRR). These techniques include the standard penetration test (SPT) and/or cone penetration test (CPT). Cyclic stress ratio (CSR) vs. CRR empirical curves were produced in the classical theory [14].

$$CSR = \frac{\tau_{avg}}{\sigma_v'} = 0.65.\frac{a_{max}}{g}.\frac{\sigma_v}{\sigma_v'}.r_d \tag{2}$$

where, a_{max} = peak ground acceleration (PGA); σ_v, σ'_v = total and effective vertical stress; r_d = depth reduction factor [15]. Furthermore, the CRR is a function of the physical properties (fines content (FC); uniformity coefficient (C_u); curvature coefficient (C_c) where they are depended on grain size parameter from laboratory sieve analysis (D_{10}; D_{30}; D_{60}; and D_{50}), magnitude (M), and value $(N_1)_{60}$ [16]:

$$CRR = h\,[f, D_{50}, M, (N_1)_{60}] \tag{3}$$

CRR value can be obtained through field testing, such as the SPT or CPT [17]. The soil will liquefy if CSR > CRR or a comparison between the CSR and CRR values as a safety factor (SF), shown in the following equation:

$$SF = \frac{CRR}{CSR} \tag{4}$$

This SF can be stated that: The SF > 1.0, the liquefaction will not occur, and the SF < 1.0, the liquefaction will occur.

3. RESEARCH METHOD

The characteristics, advantages, limitations, and specific applications of the liquefaction analysis methods have been developing. Generally, it can be summarized as follows, along

with a review of theoretical analyses and experimental results (laboratory, field, and centrifugal). For clarity, it can organize them from the most empirical to the most mechanistic/theoretical.

The simplified method [18] until present, utilizing SPT ($N_{1(60)}$), CPT ($q_{c1}N$), and V_s (V_{s_i} or shear wave velocity) based data, has been described in terms of its fundamental theory previously. This theory was developed from post-earthquake based on field observations. This semi-empirical theory is not only practical but also the most widely used in the world. It is appropriate for preliminary investigations and engineering design, having been validated by many significant earthquakes. Nonetheless, this theory has its limitations and relies heavily on the quality of field data. This theory is less affected by factors such as earthquake duration, waveforms, and complex stress paths, which typically necessitate corrections using MSF, K_σ, etc.

Several energy-based methods (energy dissipation approaches) have been developed for liquefaction occurrence when accumulated seismic energy exceeds the shear strength capacity [19]. This theory employs the following parameters, such as cyclic strain energy, cyclic intensity, etc. The advantage of this theory depends on earthquake durations, such as liquefaction caused by megathrust earthquakes, particularly in the case of long-duration (subduction).

Methods that link liquefaction to critical cyclic shear strains based on strain typically rely on laboratory experiments involving cyclic triaxial and cyclic simple shear [20]. This theory aids in understanding the behavior of enduring soil deformation. Nonetheless, it has the drawback that measuring the magnitude of strain in the field is difficult, which diminishes its practicality for routine design.

The effective stress-based and stress-path-based methods are defined by their application in soil mechanics theory [21], which includes increasing pore pressure, decreasing effective stress, and accounting for cyclic stress paths. This theory is the most consistent and has physical advantages because it is fundamentally derived from the liquefaction mechanism. Its limitations, however, include the necessity for detailed soil parameters and analyses that are relatively complex.

Advanced Constitutive Models (such as PM4Sand, UBCSAND, NorSand, and SANISAND) [22] are defined by the use of nonlinear constitutive equations, modeling the generation of pore pressure, conducting strain-softening analysis, and accounting for dilation and contraction. This theory can simulate liquefaction and post-liquefaction deformation, making it highly adaptable to different earthquake conditions. It does have limitations, though, including complex parameter calibration and sensitivity to numerical assumptions.

Various laboratory experimental methods (cyclic triaxial tests, cyclic simple shear, torsional shear, and centrifugal modeling) [23] are employed to control stress and strain conditions while directly observing pore pressure generation. One aspect of developing liquefaction theory involves laboratory work, and a benefit of this theory is that it allows for direct measurements of soil parameters. However, there are several limitations, including the small scale, which affects the sample size and disturbance effects. It is challenging to replicate the actual in-situ stresses. This is a result of the small-scale physical model being subjected to high accelerations.

The last method is a hybrid and probabilistic-based approach [24, 25]. It integrates empirical, numerical, and statistical techniques along with a framework. This approach is advantageous because it takes uncertainty into account and is appropriate for risk-based design, such as in infrastructure risk management analysis. Nonetheless, this approach has drawbacks: it necessitates a large database; it is overly complicated for everyday practice; and it requires tools tailored to contemporary seismic microzoning.

This paper used the classic simplified method by considering GSD data as a study to evaluate liquefaction in detail. All GSD data are represented on Tsuchida (1970) charts, considering all facets of seismicity, including PGA, seismicity history, etc. The selection method for conducting this research is based on laboratory and field test data (SPT; CPT) from a case study at Langsa, Indonesia. The research flowchart is shown in Figure 1. The determination of PGA relies on the earthquake model that frequently occurs at the studied location.

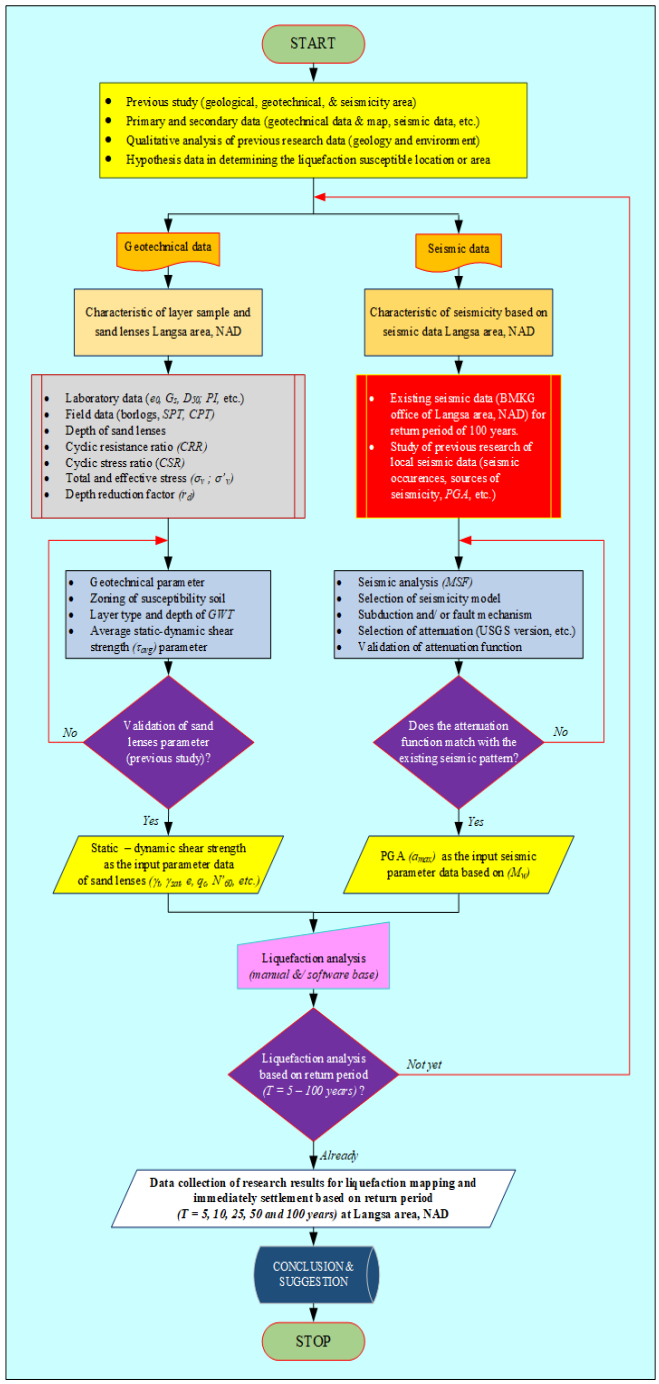

Figure 1. Flowchart of the research implementation

Based on Figure 1, in the simple methods for evaluating liquefaction, grain size and FC are crucial as they influence pore pressure formation, relative density, and the resistance of soil to cyclic loading. To sum up, their impact is reflected in the CRR value in relation to the CSR. The simple methods propose the theory that clean sand and low-silt sand are the most susceptible to liquefaction. A presumption in this study is that the presence of fine grains (silt) in low-permeability sand lens layers at depths of 2.0 to 10.0 m will lead to a faster accumulation of pore pressure during an earthquake, indicating the impact of grain size on the liquefaction mechanism. It is estimated that pore pressure will dissipate quickly and be more resistant in layers greater than 10.0 m. Fine and clean sand lenses have a loose structure and density, are susceptible to volume contraction, and rapidly lose effective stress. The fundamental theory uses clean sand as the basis of GSD, so that sand lenses mixed by silt with FC less than or < ± 35% must be corrected by the equivalent value of clean sand. The greater of the FC closing to a specific limit can be the greater of the CRR. But if the FC is excessively high and plastic, the mechanism does not involve liquefaction. Pore pressure builds up during an earthquake, which can decrease the effective stress to reach zero and cause liquefaction.

Rock weathering induces both chemical and physical transformations in the rock mass [26]. Generally, sand lenses form during the deposition of sediments, not from the weathering of solid sedimentary rock [27]. They are primary sedimentary structures, deposited by shifting energy conditions in environments like rivers, lakes, or deltas. Weathering contributes sand particles before deposition, but sand lenses themselves are a product of how and where those sands get deposited. Formation of sand lenses at the depositional origin occurs within soft, unconsolidated sediments, before the materials turn into rock. They are often the result of temporary increases in flow energy in environments dominated by finer materials, like a stream or flood that briefly deposits sand within mostly clay or silt layers. These sand patches get buried, isolated, or separated by a soft clay or silt layer, forming lens-shaped sand bodies.

Generally, sand lenses predicted to be disturbed during liquefaction are found at depths ranging from less than 10 m or 30 feet; they are submerged in water or water-saturated conditions. The susceptibility of sand lenses is the focus of this research. Liquefaction will destroy infrastructure and result in abrupt settling or land subsidence. According to observations made by the Langsa Meteorology, Climatology, and Geophysics Agency (BMKG), the Anjak Langsa fold-fault belt structure may be the source of ground shaking.

Colected of physical and mechanical properties data, at least it must cover several important things [28], including: GSD where soil layers consisting of fine sand tend to exhibit a greater level of susceptibility to liquefaction than soil layers consisting of coarse sand/gravel or silt/clay; relative density and void ratio where soil layers consisting of loose sand will liquefy more easily than dense sand (from dense sand to very dense sand); initial confining pressure and final confining pressure due to cyclic loading; intensity of surface vibrations (ground shaking) where the longer the vibrations occur, the greater the possibility of liquefaction occurring, the minimum vibration time limit is around 7 minutes; Pore water pressure can be predicted and/or measured in a soil mechanic laboratory or on-site directly, and earthquake data can be used to calculate PGA, using the point and/or gross source methods at a minimum return period (T) of 50 years.

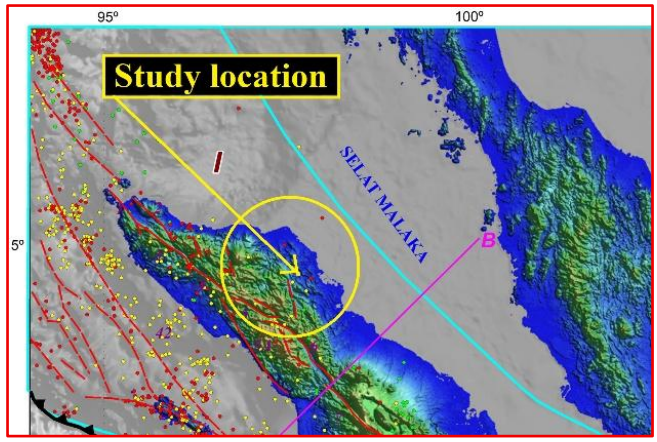

Figure 2. Earthquake map showing subduction and fault source zones (where M > 5.0) used in the hazard model

The ground motion hazard for Sumatra and the Malaysian peninsula has produced general earthquake data, which is then computed in a probabilistic framework utilizing methods created for the U.S. National Seismic Hazard Maps [29]. Regional earthquake source models used standard published and modified attenuation equations to calculate PGA at 2% and 10% probability of exceedance in 50 years for rock site conditions, as shown in Figure 2. Existing data supporting earthquakes has been processed by the active movement mechanism of fold-faults [30] because the Sumatran faults are shown close to the research area in Figure 2. It was evaluated probabilistically against the longitude-latitude coordinate parameters, maximum magnitude, hypocenter distance, and epicenter depth according to the year of occurrence or the time period (T), which was taken to be related to the existing study area. The location or study area is shown in Figure 2. The Langsa area is located in the east of Aceh Province. The area is located in the North of Sumatra Island, namely at 04° 24' 35.68" - 04° 3 3' 47.03" North Latitude and 97° 53' 14.59" – 98° 04' 42.16" East Longitude, with administrative area boundaries to the North with East Aceh zone and the Malacca Strait, to the South with East Aceh zone and Aceh Tamiang area, to the West with East Aceh zone, and to the East with Aceh Tamiang area.

4. RESULTS AND DISCUSSION

Susceptible layers in Langsa, predicted due to liquefaction phenomena from the ground surface to a depth of 10.0 m (or 30 ft), are shown in Table 1. General subsurface soil conditions are taken from field and laboratory soil investigation results. However, at a certain depth, silt clay was found in medium firm (or medium stiff) at a 4.0 to 5.0 m depth. Then, silty sand was found in loose condition at a depth of 5.00 to 8.50 m. The average of the groundwater table existed at a depth of 1.00 m. According to the existing elevation, the hard soil layer was obtained from CPT data at 27.80 m to 29.00 m depth. While GSD serves for the qualitative identification of liquefaction potential, design choices must rely on in-situ test parameters (SPT, CPT, V_s). Based on a field engineering perspective, sand lenses that require priority evaluation are: fine to medium sand; silty sand with an FC of ± 5–35%; and non-plastic silt (low PI). In addition, fine grains affect the interpretation of field test results, but do not negate the necessity for such tests. Interpretation hinges on fine content

and plasticity. It remains essential to adopt a conservative approach in areas of high seismic activity.

Table 1. General subsurface soil conditions in the study area of Langsa

Depth (m)	Soil Description
0.00 – 4.00	Near the ground surface was an organic silty clay layer with gray to blackish gray colour and very soft to soft condition. N-SPT value ranged from 3 to 4 blows, and a cone resistance (q_c) of cone penetration test (CPT) value of 2 to 8 kg/cm^2.
4.00 – 10.00	Layers consisted of sandy clayey silt in medium to stiff conditions. N-SPT value ranged from 5 to 8, and a q_c value of 8 to 15 kg/cm^2.

Lenses and thin, discontinuous layers of loose sand were commonly found in saturated clay deposits in parts of the Langsa, which are susceptible to earthquakes. These sand lenses were features that were hard to find, even after numerous test borings. They were not frequently considered in liquefaction evaluations of possible locations for engineering infrastructures, and they were challenging to find during soil examination [31]. As a result, not much research has been done on how the liquefaction of sand lenses affects the surrounding ground and any structures above them [32]. However, a number of sources have long hypothesized that the behavior of sand lenses in saturated clay deposits can have a significant impact when these lenses react in the event of an earthquake.

Grain size can be used to determine the liquefaction potential; these data could be plotted or displayed in the Tsuchida graphic [33]. These findings produced a soil grain distribution curve that can be used to calculate the prediction of liquefaction. The distribution of grain sizes for the most possibly liquefiable soil was found at the boundaries after being plotted on the Tsuchida graphic. The silt content of sandy soil or a mixture of sand and silt was ascertained by analyzing the GSD test results. A combination of silt and/or clay soil and fine sandy soil results from grain size analysis. The plotting of the grain size curve is shown in Figure 3.

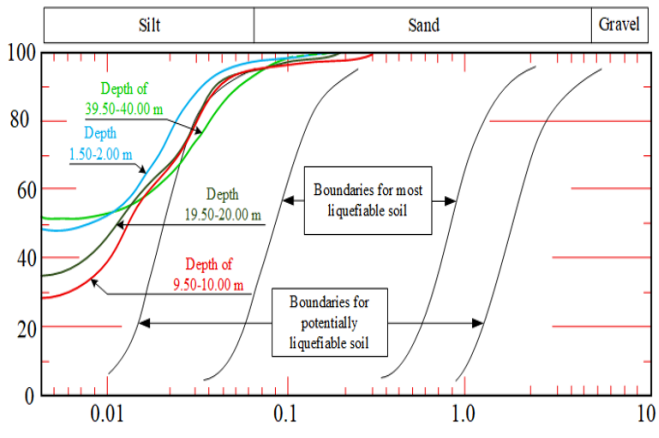

Depth location (m)	Cu	Cc	Classification	Group name
1.50-2.00	9	0.11	SW-SC	Well graded with clay
9.50-10.00	13	0.31	SW-SM	Well graded sand with silt
19.50-20.00	8	0.13	SW-SM	Well graded sand with silt
39.50-40.00	0.6	0.17	SP-SC	Poorly graded sand with clay

Figure 3. Liquefiable soil in the existing area based on the grain size analysis from Tsuchida's graphic (1970)

Generally, the observation from the plotted results shows that the 9.50 to 10.0 m depth is classified as the most liquefiable soil layer and, in USCS classification, can be indicated as SW-SM soil. However, the potential liquefaction must be proven by an analysis of CSR and CRR in order to determine the SF. The GSD of the curvature coefficient (C_c = 1) was well-graded [34]. Since the GSD was restricted to small sizes due to the curvature coefficient value (C_c < 1), it was referred to as a soil void of a complete grain size variation (gap graded). As seen in Figure 4, which is marked by the red shading, the variation of well-graded sand with silt soil demonstrates the limit of very potential for liquefaction when the sand soil contains silt particles and finer particles smaller than 0.074 millimeters passing No. 200 (US Sieve Analysis Standard) with FC > 10%. The results of the plot between parameters are shown in Figure 4.

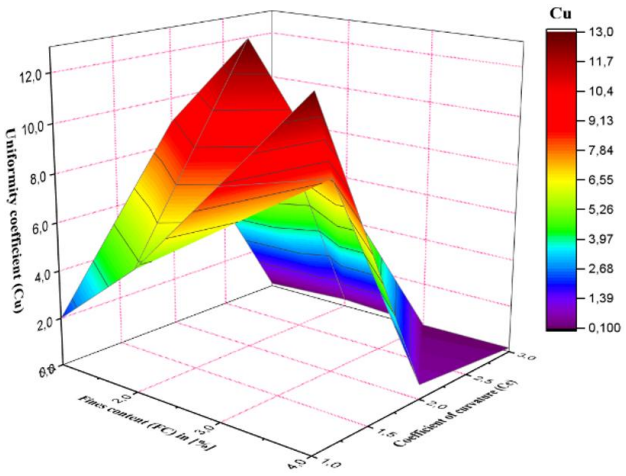

Figure 4. Uniformity coefficient (C_u) and fines content (FC) measured by the curvature coefficient (C_c)

The current correlation between the FC, C_u, and C_c of sand lenses is obtained through laboratory sieve examination, as illustrated in Figure 4. The sandy soil is well-graded, as shown by the higher C_u value. The sandy soil is of poor grade, as shown by the C_u value of less than 4. In this case, the higher the value of the FC, the higher the C_u value of the sandy soil. The graph indicates that an FC of 2% or above would have a C_c of less than 1.0. It is evident from the value of the void ratio (e) that the relative density of the soil will be impacted by the FC [35].

Table 2. Summary of CSR, CRR, and SF for T = 50 years at the depth of (9.50 – 10.00 m) (SW-SM)

Sand Lenses Location [m]	Cyclic Stress Ratio (CSR)	Cyclic Resistance Ratio (CRR)	Safety Factor (SF)
1.50 – 2.00	-	-	-
9.50 – 10.00	0.138 – 0.151	0.139 – 0.158	≤ 1.0
19.50 – 20.00	0.067 – 0.074	0.130	≥ 1.0
39.50 – 40.00	0.066	0.131	≥ 1.0

Pure sand and fine soil (e.g., silt) will affect the value of the unit weight of the soil in dry conditions. Adding fine soil content in the poorly graded sand grains will decrease the (e) value and increase dry density [36]. The point and gross source approaches were used to determine the ground surface's PGA,

also known as a_{max}, for variations in the return period. The earthquake map in this guideline includes a PGA map and the spectral response of 0.2 seconds and 1.0 seconds acceleration in bedrock (SB). Earthquake forces shall be assumed to act from all lateral directions. Appropriate response modification factors shall be used in both directions of the orthogonal axes of the substructure [37]. The N-SPT corrected value, also known as $N_{1(60)}$, and the cone resistance (q_c) value from CPT are used to determine the CRR value. The magnitude scaling factor (MSF) was used to adjust these CRR values after calibrating them against a local earthquake of magnitude 5.1 (Mw). All CSR, CRR, and SF values are shown in Table 2. Specifically for depths of 1.50 to 2.00 m, no further consideration is required, apart from being close to the ground surface, and usually the foundation is more than 2.0 m embedded.

Table 2 and Figure 5 show that the silty sand (SW-SM) has an SF above 1.0, so that theoretically it is stated that it has no potential to experience liquefaction under earthquake conditions with a magnitude of 5.1 (Mw) and an acceleration of 0.20 g [38]. The liquefaction resistance (CRR) of sand lenses may be impacted by the FC. However, CRR modifications must be made without considering the FC characteristics (such as grain sizes and plasticity), which do not accurately reflect the impact of fines on the liquefaction resistance.

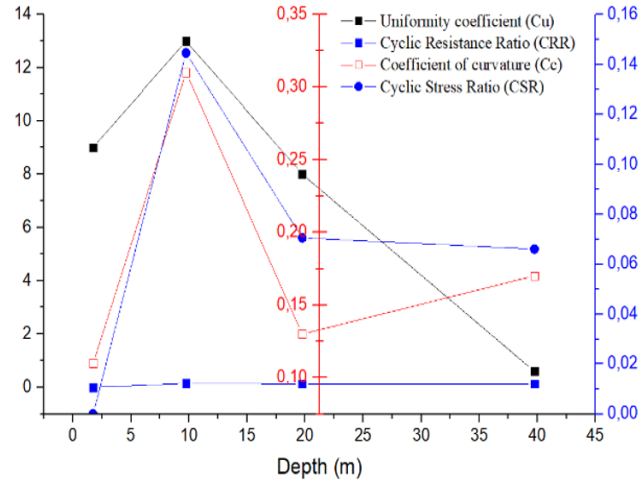

Figure 5. C_u, C_c, CSR, and CRR parameters in determining the safety factor (SF) for sand lenses location

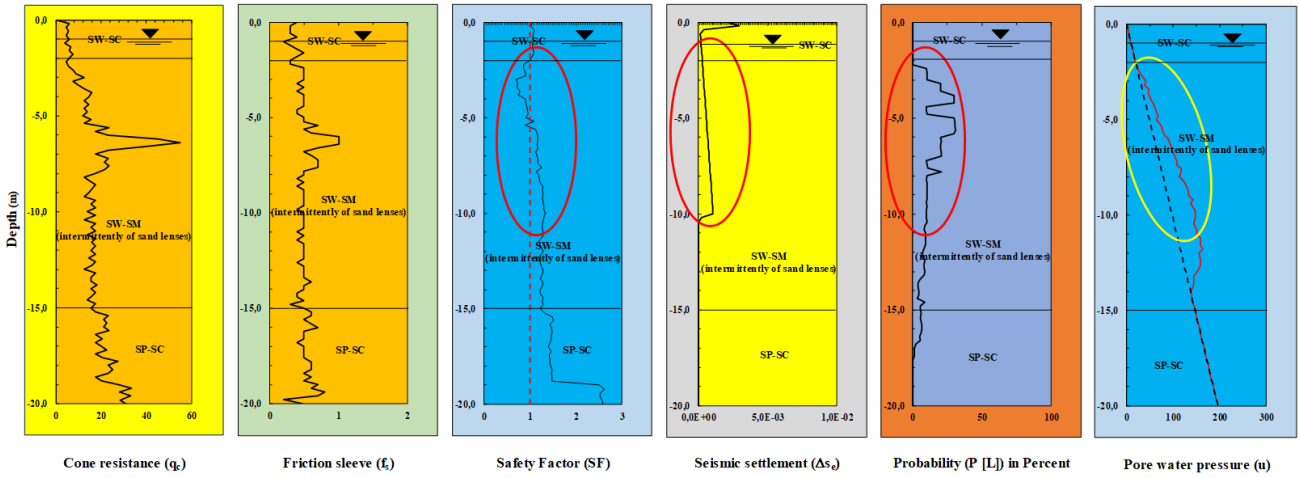

Figure 6. Safety factor (SF), seismic settlement (ΔS_e), probability of liquefaction (P[L]), pore water pressure (u) during liquefaction

Figure 6 shows the plotting results from liquefaction analysis in determining SF, seismic settlement (ΔS_e), and P[L]. The SF value ranged from 0.66 to 1.49 at depths of 2.0 to 10.00 m. Liquefaction susceptibility illustrates the relationship between soil strength and load stress, with SF < 1.0 denoting soil that is susceptible to liquefaction occurrence [39]. Correlation from the SF yielded the one-dimensional seismic settlement (ΔS_e) calculated based on CPT data, with the assumption of V_s passing through these susceptible layers of sand lenses from some literature. New models of P[L] were used with some consideration of input parameter uncertainty [40]. The P[L] for different SF values, as shown in Figure 6, it can be seen that even for SF > 1.0, the average P[L] is approximately 20%.

The prediction of pore water pressure was calculated by the formation and accumulation of excess pore pressure [41]. Even though the P[L] is below 50%, the prediction of pore water pressure can increase during liquefaction. Several variables are among the limitations of research. First and foremost, the analysis may not adequately represent changing geological conditions because it mainly uses soil investigation data from 2020. Predicting actual liquefaction events involves inherent uncertainty due to the use of a semi-empirical approach, including the fundamental theory.

Furthermore, the complicated reality of soil variability is oversimplified by the assumption that the soil parameters within boreholes are uniform [42]. Calculating magnitude and return duration based on seismic codes and historical earthquake data might not account for all possible earthquake scenarios. The lack of real-time monitoring of seismic activity, groundwater levels, and soil conditions further constrains the study of soil capacity to offer a thorough evaluation.

5. CONCLUSIONS

Generally, sand lenses in layered soils exhibit highly sensitive behavior to dynamic loads. During liquefaction, this will result in a decrease in the SF; an increase in the seismic settlement (ΔS_e) and pore water pressure (u) will increase rapidly, causing a loss of shear strength and significant local deformation. In a specific case, at a depth of 2.0 to 10.0 m, the

SF value is 0.66 to 1.49; ΔS_e is between 2.12 and 88.07 mm; u_{pre} reaches to 35% from hydaustatic pressure. However, there is a 30% chance that the sand lens layer at that location will experience liquefaction if an earthquake occurs under certain conditions. During an earthquake, saturated sand lenses trapped between impermeable layers exhibit a high tendency to experience increased pore water pressure, leading to liquefaction. This phenomenon can reduce local soil stability and act as a weak plane, triggering deformation or damage to overlying structures. In an earthquake with a 30% P[L], the sand lens layer exhibits moderate susceptibility to liquefaction. During shaking, pore water pressure increases, which partially reduces the effective stress, causing the layer to undergo local or partial liquefaction. Consequently, the shear strength of the sand lenses is reduced, and settlement or limited deformation may occur, although not to the point of complete failure.

GSD is useful for qualitatively determining the liquefaction potential, but design decisions should be based on in-situ testing parameters (SPT, CPT, V_s). Considering field engineering, the sand lenses that need priority evaluation are: fine to medium sand; silty sand with an FC of ± 5–35%; and non-plastic silt (low PI). Moreover, while fine grains influence the interpretation of field test results, they do not eliminate the need for these tests. In this instance, there is a positive correlation between the fine content and the C_u value of the sandy soil. The graph shows that if the FC is more or less 2%, the value of C_c will be under 1.0. Interpretation depends on the fine content and plasticity. In regions with significant seismic activity, it is still crucial to take a conservative approach.

ACKNOWLEDGMENTS

The author gratefully acknowledges the financial support provided by the Research and Community Service Center (P3M), Politeknik Negeri Jakarta, under Contract No. 393/PL3.A.10/PT.00.06/2025.

REFERENCES

[1] Jalil, A., Fathani, T.F., Satyarno, I., Wilopo, W. (2021). Liquefaction in Palu: The cause of massive mudflows. Geoenvironmental Disasters, 8(1): 21. https://doi.org/10.1186/s40677-021-00194-y

[2] Seed, H.B. (1982). Ground motions and soil liquefaction during earthquakes. Earthquake Engineering Research Insititue.

[3] Lee, C.J., Hung, W.Y., Tsai, C.H., Tu, Y.C., Huang, C.C., Wu, Y.C., Hsieh, M.H. (2015). Seismic responses of short grouped-piles embedded in liquefiable sandy soils during earthquakes. GEOMATE Journal, 8(16): 1218-1225. https://doi.org/10.21660/2015.16.4141

[4] Buhay, D.J.L., Legaspi, C.J.M., Perez, J.S., Lagunsad, K.D.B., et al. (2024). Mapping and characterization of the liquefaction impacts of the July and October 2022 earthquakes in Northwestern Luzon, Philippines. Engineering Geology, 342: 107759. https://doi.org/10.1016/j.enggeo.2024.107759

[5] Bol, E., Özocak, A., Sert, S., Çetin, K.Ö., Arslan, E., Kocaman, K., Ayhan, B.U. (2024). Evaluation of soil liquefaction in the city of Hatay triggered after the February 6, 2023 Kahramanmaraş-Türkiye earthquake sequence. Engineering Geology, 339: 107648. https://doi.org/10.1016/j.enggeo.2024.107648

[6] Agung, P.A.M., Ahmad, M.A. (2014). Potential liquefaction of loose sand lenses: Case study in Surabaya east coastal plain, Indonesia. International Journal of Integrated Engineering, 6(2): 1-10. https://publisher.uthm.edu.my/ojs/index.php/ijie/article/view/938.

[7] Lu, C.W., Chu, M.C., Ge, L., Peng, K.S. (2020). Estimation of settlement after soil liquefaction for structures built on shallow foundations. Soil Dynamics and Earthquake Engineering, 129: 105916. https://doi.org/10.1016/j.soildyn.2019.105916

[8] Yi, F. (2010). Procedure to evaluate liquefaction-induced settlement based on shear wave velocity. In 9th US National and 10th Canadian Conference on Earthquake Engineering 9USN/10CCEE, Toronto, Canada. https://geoadvanced.com/wp-content/uploads/2015/10/02-2010EQconf_Vs_based_liquefaction-induced_settlement.pdf.

[9] Agung, P.A.M., Ahmad, M.A., Hasan, M.F.R. (2022). Probability liquefaction on silty sand layer on central Jakarta. International Journal of Integrated Engineering, 14(9): 48-55. https://doi.org/10.30880/ijie.2022.14.09.007

[10] Dobry, R. (1982). Prediction of pore water pressure buildup and liquefaction of sands during earthquakes by the cyclic strain method. US Department of Commerce.

[11] Zhang, G., Robertson, P.K., Brachman, R.W. (2002). Estimating liquefaction-induced ground settlements from CPT for level ground. Canadian Geotechnical Journal, 39(5): 1168-1180. https://doi.org/http://doi.org/10.1139/t02-047

[12] Seed, R.B., Cetin, K.O., Moss, R.E., Kammerer, A.M., et al. (2003). Recent advances in soil liquefaction engineering: A unified and consistent framework. In Proceedings of the 26th Annual ASCE Los Angeles Geotechnical Spring Seminar: Long Beach, CA. https://digitalcommons.calpoly.edu/cenv_fac/8.

[13] Agung, P.A.M., Sultan, R., Idris, M., Sudjianto, A.T., Ahmad, M.A., Hasan, M.F.R. (2023). Probabilistic of in situ seismic soil liquefaction potential based on CPT-data in Central Jakarta, Indonesia. International Journal of Sustainable Construction Engineering and Technology, 14(1): 241-248. https://doi.org/10.30880/ijscet.2023.14.01.021

[14] Kajihara, K., Okuda, H., Kiyota, T., Konagai, K. (2020). Mapping of liquefaction risk on road network based on relationship between liquefaction potential and liquefaction-induced road subsidence. Soils and Foundations, 60(5): 1202-1214. https://doi.org/10.1016/j.sandf.2020.07.007

[15] Yoshimi, Y., Tokimatsu, K., Hosaka, Y. (1989). Evaluation of liquefaction resistance of clean sands based on high-quality undisturbed samples. Soils and Foundations, 29(1): 93-104. https://doi.org/10.3208/sandf1972.29.93

[16] Kramer, S.L., Stewart, J.P. (2024). Geotechnical Earthquake Engineering. CRC Press. https://doi.org/10.1201/9781003512011

[17] Jefferies, M., Been, K. (2015). Soil Liquefaction: A Critical State Approach. CRC Press. https://doi.org/10.1201/b19114

[18] Seed, R.B. (2010). Technical review and comments: 2008 EERI monograph, 'Soil liquefaction during earthquakes'. Geotechnical Rep. No. UCB/GT-2010, 1. https://vulcanhammer.net/wp-content/uploads/2017/01/liquefactionreview.pdf.
[19] Kokusho, T. (2013). Liquefaction potential evaluations: Energy-based method versus stress-based method. Canadian Geotechnical Journal, 50(10): 1088-1099. https://doi.org/10.1139/cgj-2012-0456
[20] Schneider, J.A., Moss, R.E.S. (2011). Linking cyclic stress and cyclic strain based methods for assessment of cyclic liquefaction triggering in sands. Géotechnique Letters, 1(2): 31-36. https://doi.org/10.1680/geolett.11.00021
[21] Lambe, W.T. (1967). Stress path method. Journal of the Soil Mechanics and Foundations Division, 93(6): 309-331. https://doi.org/10.1061/JSFEAQ.0001058
[22] Sottile, M.G. (2024). A comparison of advanced constitutive models to evaluate flow liquefaction of upstream raised tailings dams. In Proceedings of the 17th Pan-American Conference on Soil Mechanics and Geotechnical Engineering (XVII PCSMGE), La Serena, Chile. https://www.issmge.org/uploads/publications/84/130/Mauro_Giuliano_Sottile.pdf.
[23] Nong, Z.Z., Park, S.S., Lee, D.E. (2021). Comparison of sand liquefaction in cyclic triaxial and simple shear tests. Soils and Foundations, 61(4): 1071-1085. https://doi.org/10.1016/j.sandf.2021.05.002
[24] Kumar, D.R., Samui, P., Burman, A. (2022). Prediction of probability of liquefaction using hybrid ANN with optimization techniques. Arabian Journal of Geosciences, 15(20): 1587. https://doi.org/10.1007/s12517-022-10855-3
[25] Gupta, T., Ramana, G.V., Elgamal, A. (2023). A hybrid numerical–probabilistic approach for machine learning-based prediction of liquefaction-induced settlement using CPT data. Arabian Journal of Geosciences, 16(6): 394. https://doi.org/10.1007/s12517-023-11500-3
[26] Hasan, M.F.R., Frastika, M.Y., Agung, P.A.M., Susilo, A., et al. (2024). Influence of rock weathering and saturation on compressive strength and slope stability: A uniaxial test analysis. International Journal of Safety and Security Engineering, 14(1): 145-153. https://doi.org/10.18280/ijsse.140114
[27] Kessler, T.C. (2012). Hydrogeological Characterization of Low-permeability Clayey Tills: The Role of Sand Lenses. DTU Environment.
[28] Holchin, J.D., Vallejo, L.E. (1995). The liquefaction of sand lenses due to cyclic loading. In the 3rd International Conference on Recent Advances in Geotechnical Earthquake Engineering and Soil Dynamics, pp. 253-259. https://scholarsmine.mst.edu/icrageesd/03icrageesd/session03/14.
[29] Petersen, M.D., Dewey, J., Hartzell, S., Mueller, C., Harmsen, S., Frankel, A., Rukstales, K. (2004). Probabilistic seismic hazard analysis for Sumatra, Indonesia and across the Southern Malaysian Peninsula. Tectonophysics, 390(1-4): 141-158. https://doi.org/10.1016/j.tecto.2004.03.026
[30] Sathiakumar, S., Barbot, S., Hubbard, J. (2020). Earthquake cycles in fault-bend folds. Journal of Geophysical Research: Solid Earth, 125(8): e2019JB018557. https://doi.org/10.1029/2019JB018557
[31] Agung, P.A.M., Pramusandi, S., Pradiptiya, A., Adinegara, A.W., et al. (2025). Expansive residual soil stability behavior during wetting and drying process. International Journal of Safety & Security Engineering, 15(1): 127-139. https://doi.org/10.18280/ijsse.150114
[32] Mir Mohammad Hosseini, S.M., Azadi, M. (2012). Effect of the location of liquefiable sand lenses on shallow tunnels during earthquake loading. Arabian Journal for Science and Engineering, 37(3): 575-586. https://doi.org/10.1007/s13369-012-0192-7
[33] Araujo, W., Palinginis, J., Ruiz, G. (2018). Prediction methods of liquefaction phenomenon and mitigation strategies. In 16th LACCEI International Multi-Conference for Engineering, Education, and Technology, Innovation in Education and Inclusion, Lima, United States, pp. 1-8. https://doi.org/10.18687/LACCEI2018.1.1.75
[34] Yilmaz, Y., Mollamahmutoglu, M.U.R.A.T., Ozaydin, V., Kayabali, K. (2008). Experimental investigation of the effect of grading characteristics on the liquefaction resistance of various graded sands. Engineering Geology, 100(3-4): 91-100. https://doi.org/10.1016/j.enggeo.2007.12.002
[35] Do, J., Heo, S.B., Yoon, Y.W., Chang, I. (2017). Evaluating the liquefaction potential of gravel soils with static experiments and steady state approaches. KSCE Journal of Civil Engineering, 21(3): 642-651. https://doi.org/10.1007/s12205-016-1365-9
[36] Cubrinovski, M., Ishihara, K. (2002). Maximum and minimum void ratio characteristics of sands. Soils and Foundations, 42(6): 65-78. https://doi.org/10.3208/sandf.42.6_65
[37] Mi, B., Xiang, Y. (2020). Analysis of the limit support pressure of a shallow shield tunnel in sandy soil considering the influence of seepage. Symmetry, 12(6): 1023. https://doi.org/10.3390/sym12061023
[38] Ueng, T.S., Sun, C.W., Chen, C.W. (2004). Definition of fines and liquefaction resistance of Maoluo river soil. Soil Dynamics and Earthquake Engineering, 24(9-10): 745-750. https://doi.org/10.1016/j.soildyn.2004.06.011
[39] Idriss, I.M., Boulanger, R.W. (2008). Soil Liquefaction During Earthquakes (1st ed.). USA: Earthquake Engineering Research Institute.
[40] Juang, C.H., Ching, J., Luo, Z., Ku, C.S. (2012). New models for probability of liquefaction using standard penetration tests based on an updated database of case histories. Engineering Geology, 133: 85-93. https://doi.org/10.1016/j.enggeo.2012.02.015
[41] Zhang, J., Cheng, Q., Fan, H., Dai, M., Li, Y., Wu, J., Wang, Y. (2024). A new method for evaluating liquefaction by energy-based pore water pressure models. Coatings, 15(1): 7. https://doi.org/10.3390/coatings15010007
[42] Pradiptia, A., Agung, P.A.M., Pramusandi, S., Hasan, M.F.R., Suripto, bin Zainorabidin, A., Ahmad, M.A. (2023). In-situ stabilization analyses of peaty clay soil layers using solid waste from of biomass power plant. International Journal of Design & Nature and Ecodynamics, 18(6): 1299-1313. https://doi.org/10.18280/ijdne.180603